# Real part of the heavy-ion optical potential derived from relativistic mean field theory

M. Ismail
*Physics Department, Faculty of Science, Cairo University, Giza, Egypt*

H. Abozahra
*Physics Department, Faculty of Science, Cairo University, Branch of Fayoum, Fayoum, Egypt*

(Received 24 April 1995)

An energy density derived from the relativistic mean-field theory has been used to calculate the real optical potential of $^{40}$Ca-$^{40}$Ca nuclei at different energies. We used two sets of mean-field parameters which correctly produce the binding energy and saturation density of nuclear matter. We studied the effect of the relativistic corrections on the real ion-ion potential. It is found that the heavy ion potential calculated using field theory approach agrees well with that derived from nonrelativistic energy density.

PACS number(s): 24.10.Ht, 24.10.Jv, 25.70.Bc

## I. INTRODUCTION

Recently, successful attempts have been made to apply the Dirac-Brueckner-Hartree-Fock (DBHF) approach to the nuclear matter problem [1]. Unlike the nonrelativistic Brueckner-Hartree-Fock (BHF) case, the DBHF approach, due to its complexity, is much more elaborate when applied to a finite system. The existing calculations for finite nuclei either employ the nuclear matter results with some kind of local density approximation or parametrize the DBHF results for nuclear matter in terms of an effective Lagrangian which leads to the same prediction for nuclear matter as the original DBHF calculation [2]. These calculations have been extended, in the same way, to the nucleon-nucleus [3] and the nucleus-nucleus [4] scattering problems. The nucleus-nucleus interaction potential in Ref. [4] has been calculated microscopically using Dirac-Brueckner theory for nuclear matter. The effective mass of the nucleon, in these calculations, was first determined by solving the Dirac-Brueckner-Goldestone equation for nuclear matter at rest and, at the same time, the matrix elements of *NN* interaction between two nucleons in nuclear matter were obtained. These matrix elements have been used to derive a potential energy density for two colliding nuclear matter by solving the nonrelativistic Brueckner-Goldestone equation. Some authors have studied the nucleon-nucleus scattering problem using relativistic mean-field theory (RMFT) [5,6] with the Lagrangian parameterized either to reproduce the DBHF results for nuclear matter [3] or to fit the known properties of nuclear matter and some finite nuclei [7]. The nonrelativistic limit of the mean-field theory Hamiltonian is essentially equivalent to the Skyrme Hamiltonian [8] which has been quite useful in studying nuclear structure and in obtaining the real part of the nucleus-nucleus potential [9]. It may be stated that [10] relativistic mean-field models, when applied to nuclear structure, achieve about the same agreement with experiment as the density dependent interactions in the nonrelativistic Hartree-Fock approximation. The conceptual advantage is being fully relativistic and thus automatically produces the spin-orbit force which has fundamental importance in nuclear physics. After deriving the nucleon-nucleus potential using RMFT [3,7], a natural extension to the theory is to use it to derive the real part of the ion-ion potential. There are two motivations for extending the relativistic mean-field theory to the nucleus-nucleus scattering problem. The first motivation is to test if it is possible to describe nuclear matter, finite nuclei, and nuclear scattering within the same relativistic approach. The second is to assess the importance of relativistic effects on the nucleus- nucleus interaction potential.

We derive in the present work the real part of the $^{40}$Ca-$^{40}$Ca interaction potential in the frame work of RMFT. We briefly describe the mean-field method in the next section. Sections III and IV derive the real part of the nucleus-nucleus potential and discuss the relativistic effects present in the MFT. We discuss, in Sec. V, our results. Our conclusions are summarized in Sec. VI.

## II. RELATIVISTIC MEAN-FIELD APPROACH IN NUCLEAR MATTER

For symmetric nuclear matter, the Lagrangian describing the interaction of nucleons $\varphi$ with a scalar field $\sigma$ and a vector field $\omega_\mu$ is given by [7]

$$L=-\overline{\varphi}\left(\gamma_\mu\frac{\partial}{\partial\chi_\mu}+M\right)\varphi-\frac{1}{2}\left(\frac{\partial\sigma}{\partial\chi_\mu}\right)^2-U(\sigma)-\frac{1}{4}F_{\mu\nu}F_{\mu\nu}$$
$$-\frac{1}{2}m_\nu^2\omega_\mu\omega_\mu+ig_\nu\overline{\varphi}\gamma_\lambda\varphi\omega_\lambda-g_s\overline{\varphi}\varphi\sigma, \quad (1)$$

where $F_{\mu\nu}$ is the field stress tensor and

$$U(\sigma)=\frac{1}{2}m_s^2\sigma^2+\frac{1}{3}b\sigma^3+\frac{1}{4}c\sigma^4. \quad (2)$$

$M$, $m_s$ and $m_\nu$ are respectively the mass of the nucleon, scalar meson, and vector meson; $g_s$ and $g_\nu$ are the scalar and vector coupling constants.

For rotationally and translationally invariant nuclear matter, the field equations in the mean-field approximation are

$$m_s^2\sigma+b\sigma^2+c\sigma^3=-g_s\rho_s, \quad (3)$$

$$\vec{\omega}=0, \quad (4)$$

 

$$m_\nu^2\omega_0 = g_\nu \rho_\nu , \tag{5}$$

$$(-i\vec{\alpha}\cdot\vec{\nabla}+\beta M^*)\varphi_{\vec{k}} = (E-g_\nu\omega_0)\varphi_{\vec{k}} . \tag{6}$$

The positive energy solutions of the Dirac equation are the usual plane wave solutions with a reduced mass $M^* = M + g_z\sigma$. They are

$$\varphi_k \approx \begin{pmatrix} \chi \\ \dfrac{\vec{\sigma}\cdot\vec{k}\chi}{(k^2+M^{*2})^{1/2}+M^*} \end{pmatrix} \exp(i\vec{k}\cdot\overline{r}). \tag{7}$$

The source terms $\rho_s$ and $\rho_\nu$ are given as a summation of nucleons up to the top of the Fermi sphere $K_f$ where

$$\rho_s = \frac{4}{(2\pi)^3}\int^{k_f} d^3K\ \overline{\varphi_k}\varphi_k = \frac{4}{(2\pi)^3}\int^{k_f} d^3K\ \frac{M^*}{(k^2+M^{*2})}, \tag{8}$$

$$\rho_\nu = \frac{4}{(2\pi)^3}\int^{k_f} d^3K\ \varphi_k^+\varphi_k = \frac{2}{(3\pi^3)}K_f^3 . \tag{9}$$

The energy density, $e$, is given by

$$e = \tau - (M-M^*)\rho_s + \left(\frac{g_\nu}{m_\nu}\right)^2\rho_\nu^2 + U(\sigma), \tag{10}$$

where $\tau$ is given by

$$\tau = 4\int^{k_f}\frac{d\vec{k}}{(2\pi)^3}\left[\frac{k^2+MM^*}{\sqrt{k^2+M^{*2}}}-M\right]. \tag{11}$$

## III. REAL PART OF THE ION-ION POTENTIAL

We use the energy density formalism [9] to calculate the real part of the optical model potential between two nuclei. In this approach, we derive the ion-ion potential in the following way [4].

(1) We first calculate the total energy of one nucleus $E$ as

$$E = \int d\vec{r}\ \mathscr{R}(\vec{r}), \tag{12}$$

where $\mathscr{R}(\vec{r})$ is an energy density functional given by

$$\mathscr{R} = e(\rho) + H_{\rm corr}(\rho) + H_{\rm Coul}(\rho). \tag{13}$$

In Eq. (13), $e(\rho)$ is given by Eq. (10), $H_{\rm corr}(\rho)$ is a surface term of the form

$$H_{\rm corr}(\rho) = \frac{\hbar^2}{8M}\ \eta(\vec{\nabla}\rho)^2, \tag{14}$$

and $H_{\rm Coul}(\rho)$ is the Coulomb energy density. The surface strength parameter, $\eta$, is adjusted to reproduce the binding energy and rms radius of the nucleus considered. We assume the following Fermi type matter density distribution for the nucleus:

$$\rho = \frac{\rho_0}{[1+\exp(r-R_0)/a]}. \tag{15}$$

The half radius parameter $R_0$ is taken as a variational parameter to minimize the total energy of the nucleus.

(2) The real part of the nuclear potential between two nuclei is defined as the difference between their energy at distance $R$ and at infinity [9], namely

$$U(R) = E(k_r,R) - E(k_r,\infty). \tag{16}$$

$k_r$ is the distance of the centers of two Fermi spheres which represent the local densities of target and projectile nuclei. It is related to the energy of the incident particle, $E_L$ (target is assumed to be at rest), by the following equation:

$$E(k_r,\infty) = M_T + M_P + E_L , \tag{17}$$

where $M_T$ and $M_P$ are respectively the masses of the target and projectile nuclei. The total energy of the combined system $E(k_r,R)$ is obtained by integrating the Hamiltonian energy density of the combined system of the two nuclei given by

$$H^c(\rho) = H^c_{\rm corr}(\rho) + e^c(\rho), \tag{18}$$

where $\rho$ is the density of the combined system. When the two nuclei are far away the total energy is

$$E(k_r,\infty) = \int \{H^T(\rho_T) + H^P(\rho_P)\}d\vec{r}, \tag{19}$$

where $H^{T(P)}$ is the energy density of the target (projectile) nucleus given by an equation similar to Eq. (18).

In the sudden approximation, the density of the combined system is $\rho = \rho_P + \rho_T$. The kinetic energy density, $\tau(\rho)$, and the source density, $\rho_s$, of the combined system are calculated at each integration point by performing the integration over the volume of the two spheres which represent the local densities of the target and projectile nuclei at the point considered. If the two spheres overlap, the Pauli exclusion principle is taken into consideration by expanding the spheres to avoid the double occupancy region.

## IV. NONRELATIVISTIC APPROXIMATION

It should be noted that in the following section terms up to order $\rho^3$ have been kept in the energy density. As pointed out in Ref. [5], the description of this approximation as nonrelativistic is not strictly accurate since terms of relativistic origin have been kept in the energy density functional. The Hamiltonian energy density, $\mathbf{e}(\rho)$ [given by Eq. (10)] can be written as

$$e = \tau + \pi, \tag{20}$$

where $\tau$ and $\pi$ are respectively the kinetic and potential energy densities. The potential energy term of Eq. (20) can be written as

$$\pi = -(M-M^*)\rho_s + \frac{1}{2}\left(\frac{g_\nu}{m_\nu}\right)^2 \rho_\nu^2 + \frac{1}{2}\left(\frac{m_s}{g_s}\right)^2 (M^*-M)^2 + \frac{1}{3}\frac{b}{g_s^3}(M^*-M)^3 + \frac{1}{4}\frac{c}{g_s^4}(M^*-M)^4. \quad (21)$$

The fourth term in the last equation reduces in the nonrelativistic approximation to a repulsive effective three-body interaction or density dependent two-body interaction [5]. Also, it has been shown in Ref. [5] that the energy density due to exchange of scalar mesons is given by $[-(1/2)(g_s^2/m_s^2)\rho_s^2]$. In the nonrelativistic limit it is equivalent to the two terms $[-(1/2)(g_s^2/m_s^2)\rho^2 + (1/2)(g_s^2/m_s^2)(\rho\tau/M^*)]$. The second term weakens the contribution of the energy density from the scalar interaction and it has the same effect as a momentum dependent interaction [5].

## V. NUMERICAL RESULTS AND DISCUSSION

We perform our calculations, in the present work, taking the $^{40}$Ca-$^{40}$Ca scattering process as an example. We consider RMFT with two sets of parameters. The first set is that derived by Boguta and Moskowsky [5] and we call it the BM model. The second is the so-called BB (Boguta and Bodmer) model used in Ref. [7]. These two models differ largely in the value of $M^*/M$. While for the BM model $M^*/M \approx 0.7$ at the saturation density of nuclear matter, its value is 0.935 for the BB model.

Figure 1 shows the difference in the kinetic energy between the composite and separate systems. $U_\tau$, for two values of the relative momentum, $k_r$. For the BM model, this difference is strongly attractive at small values of the separation distance $R$. This is due to the kinetic energy of the combined system that depends on the effective mass, which becomes smaller at higher density values ($M^*/M \approx 0.7$ and 0.5 for $\rho = 0.16$ and 0.32 fm$^{-3}$, respectively). On the other hand, at an integration point $\vec{r}$, the density of the target, $\rho_T$, and that of the projectile, $\rho_P$, correspond to two spheres in momentum space which strongly overlap at small values of $k_r$. The procedure of expanding the two overlapping spheres to larger radii to avoid the double occupancy region increases the kinetic energy density of the combined system calculated at the point $\vec{r}$. This effect dominates at $k_r = 0.5$ fm$^{-1}$ and $U_\tau$ becomes positive for $R > 4$ fm. For $k_r = 3$ fm$^{-1}$, the two Fermi spheres are well separated in momentum space and the effective mass effect makes $U_\tau$ negative for all distances.

For the BB model, the effect of effective mass on $U_\tau$ is nearly absent ($M^*/M \approx 0.921$ for $\rho = 0.32$ fm$^{-3}$ and 0.937 for $\rho = 0.16$ fm$^{-3}$) and the difference in kinetic energy between the combined system and the separate system is positive at nearly all values of $k_r$. It behaves like the nonrelativistic case.

Figure 2 shows the difference in potential energy ($U_\pi$) between the composite system and separate system. $U_\pi$ contains a term which is quadratic in $\rho$ and other terms contain powers of $(1-M^*/M)$. For the BM model, where $M^*/M$ varies significantly with $\rho$, it is shown that $U_\pi$ is strongly energy dependent. It is strongly repulsive at small distances and becomes weakly attractive in surface and tail regions (as shown in Fig. 2). For the BB model where $M^*/M$ varies slowly with $\rho$, $U_\pi$ is attractive and nearly energy independent as shown in Fig. 2. The difference in $U_\pi$ between BM and BB models is due to the difference in parameters between the two models. For example, the strength of the second term of Eq. (21) for the BM model is about 40 times its strength for the BB model.

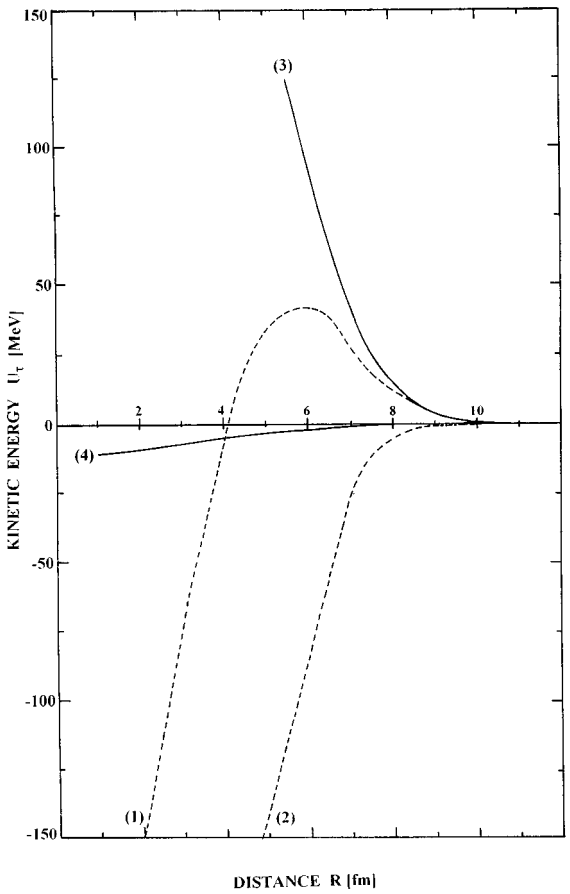


FIG. 1. The difference in the kinetic energy between the composite and separate systems for the nuclear pair $^{40}$Ca-$^{40}$Ca calculated using both BB and BM model. Dashed curves (1) and (2) correspond to the BM model with $K_r = 0.5$ and 3 fm$^{-1}$, respectively; solid curves (3) and (4) are those for the BB model with $K_r = 0.5$ and 3 fm$^{-1}$, respectively.

Figure 3 shows the contribution of $U$ from the term $[-(1/3)b(1-M^*/M)^3M^3]$ present in the Hamiltonian energy density (let us name it $U_3$). As pointed out in Sec. IV, this term reduces $(1/16)t_3\rho^3$ and it corresponds, in the nonrelativistic approximation, to the contribution of the ion-ion potential from a three-body force. The figure shows that $U_3$ is weakly energy dependent and it is repulsive for the BM model. On Fig. 3 we have also displayed the nonrelativistic approximation of $U_3$ for a value of the parameter $t_3$ that corresponds to Skyrme parameter set S III [9]. Compared with the contribution of $U$ from this term, relativistic correction makes $U_3$ less repulsive at all nucleus-nucleus separation distances $R$.

Figure 4 represents the contribution of $U$ from the energy density $[-(1/2)(g_s^2/m_s^2)\rho_s^2]$. It represents the scalar interaction energy density (as pointed out in Sec. II), which is due to the exchange of scalar mesons. In the nonrelativistic approximation it becomes $[-(1/2)(g_s^2/m_s^2)\rho^2 + (1/2)(g_s^2/$

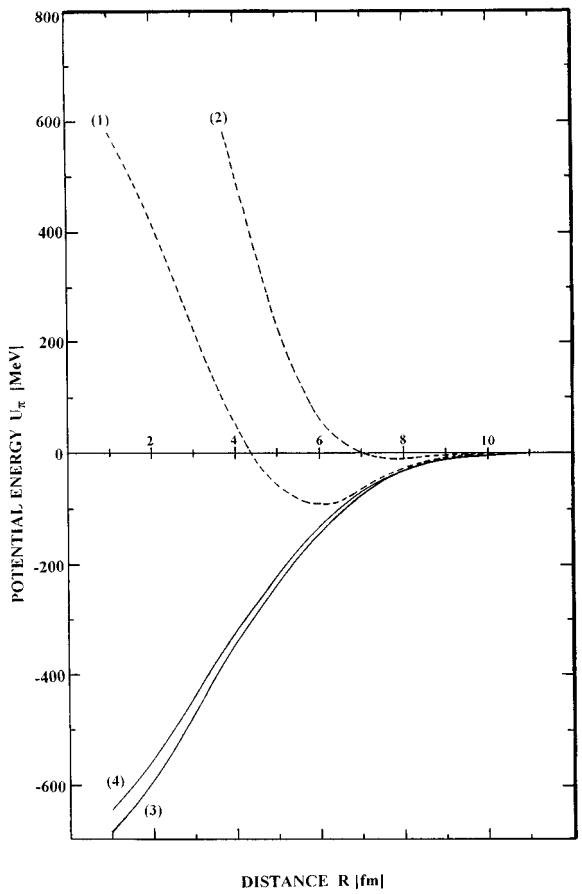


FIG. 2. The same as Fig. 1 but for the contribution of the real $^{40}$Ca-$^{40}$Ca potential from the potential energy $U_\pi$.

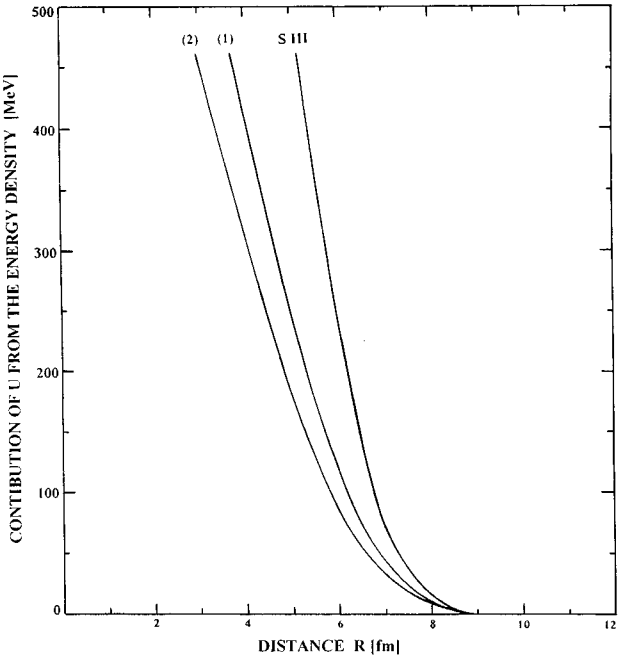


FIG. 3. Comparison between the $U_3$ term and its corresponding term in the nonrelativistic approximation ($1/16t_3\rho^3$). The comparison has been made for the nuclear pair $^{40}$Ca-$^{40}$Ca using the BM model. Curves labeled by (1) and (2) correspond respectively to $E_L/A\sim6.3$ and 197.8 MeV.

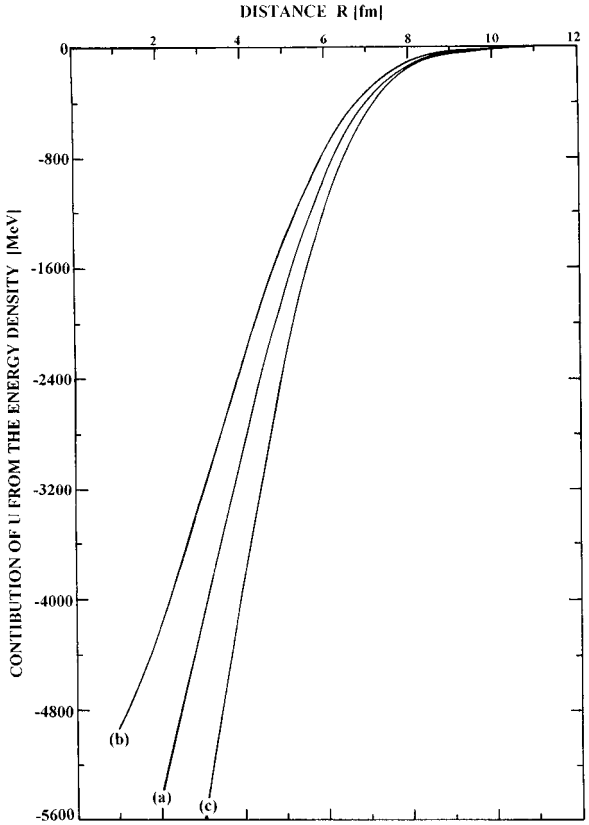


FIG. 4. Curves (a) and (b) represent the contribution of $U$ from the energy density term $[-(1/2)(g_s^2/m_s^2)\rho_s^2]$ calculated for the nuclear pair $^{40}$Ca-$^{40}$Ca using the BM model at $E_L/A\sim6.3$, 197.8 MeV. Curve (c) represents the contribution of $U$ from the nonrelativistic approximation term $[-(1/2)(g_s^2/m_s^2)\rho^2]$.

$m_s^2)(\rho\tau/M^*)]$. The second term is the relativistic weakening of the scalar density and has the same effect as a momentum dependence of the scalar interaction. As shown in Fig. 4, the effect of the relativistic weakening of the scalar density on the nucleus-nucleus potential is large and increases as the energy increases.

Figure 5 shows the total interaction potential for the nuclear pair $^{40}$Ca-$^{40}$Ca at different values of the incident energy per particle, $E_L/A$, calculated using the BM model. The ion-ion potential shows strong repulsion in the inner region. The surface and tail regions are attractive. The value of the minimum of the curve increases as the value of $E_L/A$ increases till $E_L/A\approx54$ MeV, then it starts to decrease and the curve calculated at $E_L/A\approx200$ MeV is higher than that corresponding to $E_L/A\approx6$ MeV. The shape and the energy dependence of the ion-ion potential is similar to that calculated using the Skyrme energy density [11].

Figure 6 is the same as Fig. 5 but the $^{40}$Ca-$^{40}$Ca potential has been calculated using the BB model. Except for $E_L/A\approx5.2$ MeV, the ion-ion potential derived from the BB model is strongly attractive in the inner region. In the surface and tail regions ($R>7$ fm) its value is nearly the same as that derived from the BM model for $E_L/A<100$ MeV. For greater values of $E_L/A$, it becomes more attractive in the surface region compared to that of the BM model. This is because its energy dependence decreases as $E_L/A$ becomes more than 100 MeV. The behavior of $U(R)$ calculated from

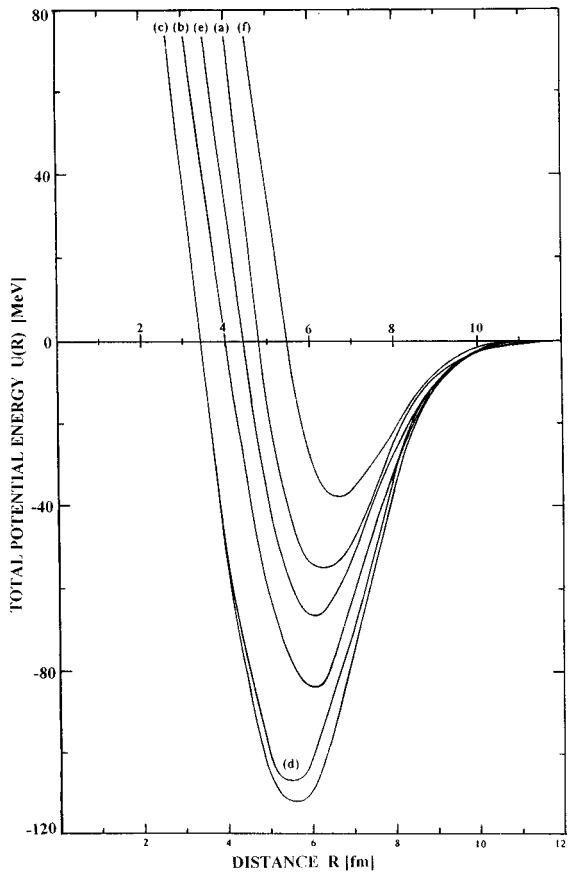


FIG. 5. The real part of the optical potential for the nuclear pair $^{40}$Ca-$^{40}$Ca calculated using the BM model. Curves labeled by (a), (b), (c), (d), (e), and (f) correspond respectively to $E_L/A \sim 6.3$, 24.8, 54.5, 94.2, 142.4, and 197.8 MeV.

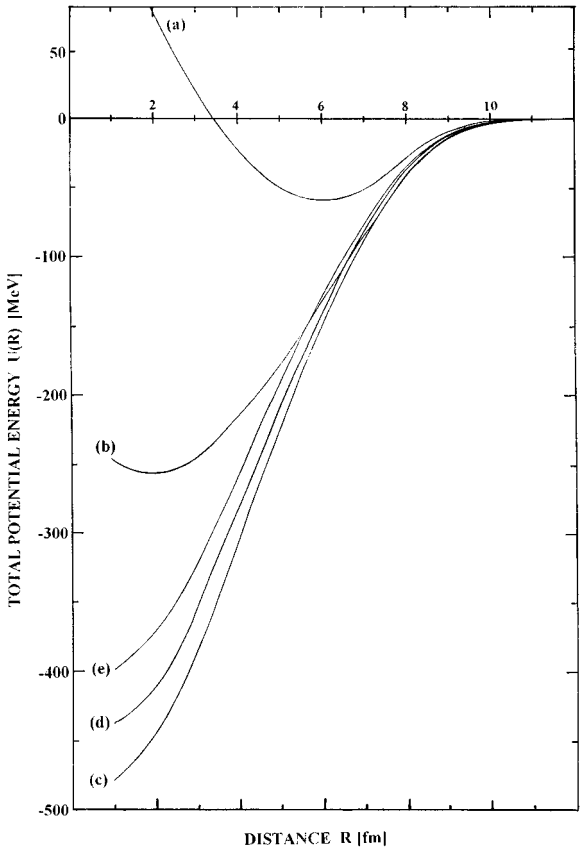


FIG. 6. The same as Fig. 5 but calculated by using the BB model. Curves labeled by (a), (b), (c), (d), and (e) correspond respectively to $E_L/A \sim 5.3$, 46.5, 124.1, 230.8, and 359.3 MeV.

the BB model can be easily understood from Figs. 1 and 2. For small values of $E_L/A$, $U_\tau$ is strongly repulsive (due to the effect of the Pauli exclusion principle) and $U_\pi$ is attractive. As $E_L/A$ increases, the contribution of $U$ from the kinetic energy density $U_\tau$ becomes smaller and since $U_\pi$ is nearly energy independent the total potential becomes attractive.

It is generally believed [12] that the heavy ion elastic scattering data fits the potential value only at the vicinity of the strong absorption radius $R_{\mathrm{SA}}$. We now compare the ion-ion potential value obtained from experiment at $R = R_{\mathrm{SA}}$ with the corresponding quantities calculated using the BM and BB models. The values of $R_{\mathrm{SA}}$ and $U(R_{\mathrm{SA}})$ are taken from Ref. [13]. Table I shows the normalization factors $N_1$ and $N_2$ required for the BM potential and the BB potential to fit the experimental data at the strong absorption radius for five pairs of interacting nuclei. Except for the heavier pair $^{40}$Ca-$^{40}$Ca the predicted potential from the BB model or from the BM model at the strong absorption radius agrees well with that extracted from experiments at low energy per projectile particle (3.8–4.7 MeV). The ion-ion potential derived from the BM model is a little bit better than that derived from the BB model. For the $^{40}$Ca-$^{40}$Ca pair, the two models predicted a weak potential that needs a factor of 1.6 in order to agree with experiment. At higher energy ($E_L/A = 44$ MeV)

TABLE I. The normalization factors $N_1$ and $N_2$ require by BM and BB potentials, respectively, to fit the experimental values at the strong absorption radius for five pairs of interacting nuclei. $N^{M3Y}$ and $N^{DDM3Y}$ are the normalization factors for the nonrelativistic potentials $M3Y$ and $DDM3Y$, respectively.

| System | $E_L$ (MeV) | $R_{\mathrm{SA}}$ (fm) | $N^{M3Y}$ | $N^{DDM3Y}$ | $N_1$ | $N_2$ |
|---|---|---|---|---|---|---|
| $^{12}$C+$^{40}$Ca | 45 | 9.0 | 1.01 | 0.70 | 0.98 | 0.89 |
| $^{12}$C+$^{40}$Ca | 51 | 9.1 | 0.92 | 0.63 | 0.91 | 0.85 |
| $^{16}$O+$^{40}$Ca | 74.4 | 9.3 | 1.03 | 0.71 | 1.06 | 1.03 |
| $^{40}$Ca+$^{40}$Ca | 143.6 | 10.7 | 0.99 | 0.64 | 1.62 | 1.60 |
| $^{40}$Ar+$^{60}$Ni | 1760 | 10.15 | 0.60 | 0.56 | 0.53 | 0.39 |
| $^{12}$C+$^{90}$Zr | 98 | 10.0 | 0.96 | 0.72 | 0.74 | 0.57 |

the two models predict a more attractive potential than that required to fit the data at $R_{SA}$. This potential should be normalized by 0.4 for BB and 0.53 for BM models. Table I contains the normalization factors $N^{M3Y}$ and $N^{DM3Y}$ needed by the nonrelativistic ion-ion real potential calculated using the well known nucleon-nucleon potentials $M3Y$ and $DDM3Y$ of Refs. [14, 15] to fit the data at the strong absorption radius. The table shows that the relativistic ion-ion potentials agree well with the nonrelativistic potentials at $R_{SA}$.

## VI. SUMMARY

We have studied the real part of the optical potential between two nuclei using relativistic mean-field theory with two sets of parameters namely; a BM model with effective mass of about 0.6 at the saturation density and a BB model whose effective mass is about unity. The two models produce the nuclear matter data and both the binding energy and rms radii of the nuclei considered. The difference in effective mass between the two models has a large effect on both the shape and energy dependence of the ion-ion potential. In the inner and surface regions of the ion-ion potential, the BB model predicts a deeper potential compared with that predicted by the BM model. At the strong absorption radius we have found that the potentials predicted by the two models agree well with those extracted from experiment for projectile energy per particle 3.8–4.7 MeV. At higher projectile energy, RMFT predicts more attractive potential than that required by experiment.

## ACKNOWLEDGMENTS

We thank Dr. Larry Slater from the American University in Cairo for his language correction support.

[1] R. Brockman and R. Machledit, Phys. Lett. **149B**, 283 (1984); R. Machledit and R. Brockman, *ibid*. **160B**, 364 (1985).
[2] H. Elsenhans, H. Muther, and R. Machledit, Nucl. Phys. **A515**, 715 (1990); R. Brockman and H. Toki, Phys. Rev. Lett. **68**, 340 (1992).
[3] G. Q. Li, R. Machledit, R. Fritz, H. Muther, and Y. Z. Zhuo, Phys. Rev. C **48**, 2443 (1993).
[4] N. Ohtsuka, M. EL Shabshiry, R. Linden, H. Muther, and A. Faessler, Nucl. Phys. **A490**, 715 (1988); M. Ismail, M. Rashdan, A. Faessler, R. Linden, N. Ohtsuka, and W. Wadia, *ibid*. **A496**, 795 (1989).
[5] J. Boguta and S. A. Moszkowski, Nucl. Phys. **A403**, 445 (1983).
[6] B. D. Serot and J. D. Walecka, Adv. Nucl. Phys. **16**, 1 (1986); P. G. Reinhard, Rep. Prog. Phys. **52**, 439 (1989); Stefan Gmuca, Nucl. Phys. **A547**, 447 (1992).
[7] J. Boguta, Phys. Lett. **106B**, 250 (1981).
[8] T. H. R. Skyrme, Philos. Mag. **1**, 1043 (1956).
[9] D. M. Brink and F. Stancu, Nucl. Phys. **A243**, 175 (1975); F. Stancu and D. M. Brink, *ibid*. **A270**, 236 (1976).
[10] P. G. Reinhard, M. Rufa, J. Maruhn, W. Greiner, and J. Friedrich, Z. Phys. A **323**, 13 (1986); Y. K. Gambhir, P. Ring, and A. Thimet, Ann. Phys. (N.Y.) **198**, 132 (1990).
[11] M. Ismail, M. Osman, Jannette W. Guirguis, Kh. A. Ramadan, and H. Abozahra, J. Phys. G **15**, 1033 (1989).
[12] G. R. Satchler, Proceedings of the International Conference on Relations between Complex Nuclei, Nashville, 1974 (unpublished), Vol. 2, p. 171.
[13] A. K. Chaudhuri and B. Sinha, Nucl. Phys. **A455**, 169 (1986).
[14] G. R. Satchler and W. G. Love, Phys. Rep. **55**, 183 (1982).
[15] A. M. Kobos, B. A. Brown, P. E. Hodgson, G. R. Satchler, and A. Budzanowski, Nucl. Phys. **A384**, 65 (1982); A. M. Kobos, B. A. Brown, R. Lindsay, and G. R. Satchler, *ibid*. **A425**, 205 (1985).